ISSN 0915-633X

NATIONAL INSTITUTE FOR FUSION SCIENCE

Suppression of Accelerated Electrons in a High-current Large Negative Ion Source

Y. Takeiri, Y. Oka, M. Osakabe, K. Tsumori, O. Kaneko,
T. Takanashi, E. Asano, T. Kawamoto,
R. Akiyama and T. Kuroda

(Received - Nov.19, 1996)

NIFS-467 Dec. 1996

RESEARCH REPORT
NIFS Series

NAGOYA, JAPAN

Suppression of accelerated electrons in a high-current large negative ion source

Y. Takeiri, Y. Oka, M. Osakabe, K. Tsumori, O. Kaneko, T. Takanashi,
E. Asano, T. Kawamoto, R. Akiyama and T. Kuroda

National Institute for Fusion Science, Nagoya 464-01, Japan

ABSTRACT

Accelerated electrons, which would lead to high thermal load of grids, have been suppressed in a high-current large hydrogen negative ion source. An aperture of the extraction grid is shaped as the secondary electrons generated on the grid aperture surface would be shielded against the acceleration electric field. The shaped aperture extraction grid works well to prevent the secondary electrons from leaking to the acceleration gap, compared with a straight aperture extraction grid. Although the strong magnetic field at the extraction grid also lowers the electron leakage downstream, the aperture shaping of the extraction grid is more effective for the suppression of the accelerated electrons. The acceleration efficiency, defined by the ratio of the negative ion current to the acceleration drain current, is improved to around 85 %. There remains the accelerated electrons generated in the negative ion neutralization by collision with the residual neutral molecules during the acceleration. The direct interception of the accelerated negative ions with the downstream grid is small. The reduction of the operational gas pressure is quite important to achieve the further improvement of the acceleration efficiency.

Keywords : negative ion source, negative-ion-based NBI, accelerated electron suppression, secondary electron leakage, grid aperture shaping, grid thermal load, acceleration efficiency, stripping loss, cesium seeding, long pulse operation

I. INTRODUCTION

Large-scaled negative ion sources have been intensively developed[1-6] for a negative-ion-based neutral beam injector (NBI) in the next step experimental fusion devices, such as ITER (International Tokamak Experimental Reactor)[7] where 1 MeV-50 MW neutral beam injection is proposed.[8] JAERI has produced 400 keV-13.5 A D^- ion beam,[9] and constructed a negative-ion-based NBI which has started the injection to JT-60U tokamak.[10] Cadarache has accelerated a H^- ion beam of 40 mA to 910 keV.[11]

In National Institute for Fusion Science (NIFS), large-scaled hydrogen negative ion sources have been developed[2-4,12-24] for a negative-ion-based NBI system[25,26] in LHD (Large Helical Device), which is a world-largest superconducting helical system.[27] Until now, 16.2 A of H^- ion beam has been obtained with a current density of 31 mA/cm^2,[4] 13.6 A of H^- ion beam has been accelerated to 125 keV,[21] and multibeamlet focusing has been achieved with a divergence angle of 9 mrad by the aperture displacement technique.[22] High-current density operation of 45 mA/cm^2 [3] and low divergence single beamlet production of 5 mrad[24] have been also achieved. However, these results have been obtained in a short pulse operation of less than 0.3 s. In the next step experimental fusion devices, long pulse and / or continuous operation is projected, and the NBI system should be operated continuously. At present, cesium-seeded volume negative ion sources are used for high-current negative ion beam production.[1,12,28,29] Stable operation of a cesium-seeded source has been demonstrated for a long pulse duration of 1000 s with a current density of 14 mA/cm^2.[30] In this case, the thermal load of the grounded grid was about 25 % of the total H^- ion beam power, and it would be difficult to remove the thermal load of the grounded grid in a long pulse operation with higher power.

The thermal load of the grounded grid is mainly ascribed to the incidence of the accelerated electrons, which are generated in the neutralization of the negative ions by collision with the residual neutral molecules or generated as the secondary electrons on the extraction (or the upstream) grid. The latter electrons must be strongly suppressed by the geometrical grid configuration while the former electrons can be suppressed by reduction of the operational gas pressure. In single beamlet or small grid area experiments, high acceleration efficiency of the negative ions has been obtained by devising the extraction-acceleration grid structure.[24,31,32] Therefore, it is important to demonstrate the suppression of accelerated electrons in a high-power large negative ion source with wide-area multiaperture grids, and to clarify the origin of the accelerated electrons.

We have measured the thermal load of the grids using a high-current large negative ion source producing 270 beamlets in an area of 25 cm$\times$26 cm, and investigated the cause of the

thermal load. A newly designed extraction-acceleration grid system is used and the accelerated electrons generated as the secondary electrons at the extraction grid were successfully suppressed. In this paper, following the description of the ion source and the grid system, the experimental results of the suppression of accelerated electrons are presented by making a comparison between two types of grid system. The origin of the accelerated electrons is also discussed.

II. EXPERIMENTAL SETUP

A. External filter type large negative ion source

A schematic diagram of an external filter type large hydrogen negative ion source is shown in Fig. 1. The high-density filament-arc plasma is generated in a multicusp bucket source, the dimensions of which are 35 cm × 62 cm in cross section and 20 cm in depth. This source is characterized by strong external magnetic filter field generated in front of the plasma grid over a wide area of 35 cm × 62 cm by a pair of permanent magnet rows facing each other at a separation of 35 cm. The central magnetic field strength is 52 G and the integrated filter field strength is 650 G cm. The detailed structure is described in ref. 4. Two cesium ovens are installed on the chamber wall for the cesium injection. The gas pressure in the arc chamber is controlled with a mass flow controller. The flow rate is converted to the gas pressure using a capacitance manometer (MKS Baratron) attached directly to the arc chamber.

The negative ion accelerator was originally designed as a five-grid two-stage accelerator, and an H^- ion beam of 16.2 A was obtained from 522 apertures in an area of 25 cm × 50 cm and 13.6 A of H^- ions were accelerated to 125 keV. In this experiment, a single-stage accelerator was used. The detailed grid arrangement is shown in the following section.

The negative ion source is attached to the negative-ion-based NBI teststand, where two large vacuum vessels are connected with a 5 m-long neutralizer.[13,15] The gas pressure in the first vessel, where the ion source is attached and a cryopump of 450 m^3/s is installed, is around 3×10^{-5} Torr in the operation. The negative ion current is measured with two-dimensional calorimeter arrays located 5 m and 11.2 m downstream. The beam pulse length is 0.6 s.

B. Grid configuration of accelerator

Two types of extraction-acceleration grid arrangement were used in the experiments. The grid arrangement with a straight aperture extraction grid is shown in Fig. 2 (a), which consists of plasma, extraction, electron suppression and grounded grids. The plasma grid is made of molybdenum and thermally insulated to keep the grid temperature over 200℃ during the

operation. The extraction grid contains permanent magnets which generate the magnetic field both upstream and downstream for electron deflection. The electrons extracted together with the negative ions are deflected by the upstream magnetic field and incident on the extraction grid. A part of the secondary electrons generated on the extraction grid would be trapped by the downstream magnetic field. The maximum magnetic field strength on the beam axis is 450 G at the room temperature in this grid arrangement. The extraction voltage is 5-10 kV and the thermal load of the extraction grid by the impinging of the extracted electrons is large and, therefore, tubes for water cooling are buried. The electron suppression grid is electrically connected to the extraction grid. The experimental results when removing the electron suppression grid (three grid system − grid arrangement A) are compared with those in four grid system (grid arrangement B). Since a part of the accelerated electrons impinge the grounded grid, the thermal load of the grounded grid is large. Therefore, tubes of 4 mm in outer diameter are silver-soldered for water cooling between aperture rows.

The grid arrangement with a shaped aperture extraction grid is shown in Fig. 2 (b), which uses the same plasma and grounded grids as those in Fig. 2 (a). The extraction grid apertures are shaped. The upstream opening is narrower than that of the extraction grid in Fig. 2 (a), and widened gradually toward the downstream. The end opening is made narrow again as the secondary electrons generated upstream would not leak to the acceleration gap. The larger permanent magnets are inserted in the extraction grid, and the maximum magnetic field strength on the beam axis is 650 G at the room temperature (grid arrangement C). The experiments where the same permanent magnets as those in the extraction grid in Fig. 2 (a) are inserted in the extraction grid in Fig. 2 (b) (grid arrangement D) are made, and the results are compared.

There are 270 apertures (18×15) of 9 mm in diameter in an area of 25 cm×26 cm on the plasma grid. The multibeamlets are focused around 12 m downstream by the aperture displacement of the grounded grid.[22]

C. Thermal load measurement by water-calorimetry

The thermal loads of the extraction grid and the grounded grid are estimated by the water-calorimetry, where the temperature difference between the water inlet and outlet and the water flow rate are measured. Figure 3 shows an example of the time evolution of the temperature difference between water inlet and outlet, i.e., the water temperature rise, of the grounded grid and the extraction grid. The beam pulse length is 0.6 s. Since the thermal capacity of the extraction grid is larger than that of the grounded grid, the time constant of water temperature rise is longer in the extraction grid. The arc discharge starts 5 s prior to the beam pulse in this

shot and the water temperature in the extraction grid starts to rise before the negative ion extraction. It is found that the thermal load of the extraction grid contains the heat from the arc discharge. The thermal powers to the extraction grid and the grounded grid estimated by the water-calorimetry are converted to the equivalent thermal load currents to the corresponding grids, Ieg and Igg, using the extraction voltage and the acceleration voltage, respectively.

III. EXPERIMENTAL RESULTS AND DISCUSSION

A. In the case of a straight aperture extraction grid

The negative ion extraction and acceleration properties are investigated for the grid arrangement with a straight aperture extraction grid as shown in Fig. 2 (a). The extraction current, Iext, the acceleration current, Iacc, and the H^- ion current, I_{H^-}, are shown in Fig. 4 (a), as a function of the arc power for the grid arrangement A. The gas pressure in the arc chamber is 3.2 mTorr. The electron suppression grid is not used. The extraction voltage, Vext, and the acceleration voltage, Vacc, are changed as the voltage ratio of Vacc/Vext is constant of around 12, in order to keep the negative ion beam optics constant. The Vacc is changed 45 - 83 kV as the arc power increases in this experiment, as shown in Fig. 4 (a). It is found that these currents increase proportionally to the arc power. Figure 4 (b) shows the equivalent thermal load currents to the extraction grid and the grounded grid, Ieg and Igg, respectively, as a function of the arc power. The thermal load currents also increase proportionally to the arc power.

The ratio of the H^- ion current to the acceleration drain current, I_{H^-}/I_{acc}, i.e., the acceleration efficiency, and the ratio of the equivalent thermal load current to the grounded grid to the H^- ion current, I_{gg}/I_{H^-}, are shown in Fig. 5, as a function of the arc power for the grid arrangement A and B. The experimental conditions are the same as those in Fig. 4. The roll of the electron suppression grid in the case of the straight aperture extraction grid is investigated. The I_{H^-}/I_{acc} and the I_{gg}/I_{H^-} are almost insensitive to the arc power and nearly the same for both grid arrangements. The acceleration efficiency, I_{H^-}/I_{acc}, is low, 60-65 %, and the I_{gg}/I_{H^-} is high, 24-25 %. These results indicate that a large number of electrons are accelerated and a part of them are incident on the grounded grid. Considering the operational gas pressure, the stripping loss of the negative ions during the acceleration is estimated to be less than 8 % of the H^- ion current. Therefore, most of the accelerated electrons should be derived from the extraction grid. The electron suppression grid would have worked as a shield against the acceleration electric field, and the secondary electrons generated at the extraction grid could not have been accelerated downward. However, the accelerated electrons are not reduced by installing the

electron suppression grid, as shown in Fig. 5. As the secondary electrons are not easily absorbed to the extraction grid, some of them probably leak to the downstream gap where the acceleration electric field exists. The secondary electrons generated at the electron suppression grid by the impinging of the H^- ions could be directly accelerated.

On the other hand, the electrons extracted together with the H^- ions are considered to be much suppressed. The thermal load of the extraction grid is small and the ratio of Ieg/Iext is about 16 %. Since the ratio of I_{H^-} /Iext is about 55 % in Fig. 4 (a), around 29 % of the extraction current leak to the acceleration gap except for the H^- ion current measured at the calorimeter array. The leakage current contains the direct loss of the H^- ion current to the grounded grid, the stripped electrons by the H^- ion neutralization and the leakage current of the secondary electrons generated without giving the power to the extraction grid by shallow incidence of the extracted H^- ions and electrons. Therefore, it is important to prevent the secondary electrons with a relatively high energy from leaking to the acceleration gap.

B. In the case of a shaped aperture extraction grid

In order to reduce the leakage of secondary electrons from the extraction grid, the extraction grid aperture has been shaped as shown in Fig. 2 (b). The upstream opening is made narrower for intercepting the distorted H^- ions of the beamlet periphery, which would strike the inner surface of the aperture. Moreover, by increasing the magnetic field for the electron suppression (the grid arrangement C), almost all of the extracted electrons should be incident on the upstream surface with the narrow opening of the extraction grid. The inner diameter of the aperture is gradually wider toward the downstream, and the end opening is narrowed down again. The energetic secondary electrons generated on the inner surface of the aperture would be trapped at the depression. The narrow end aperture also works as a shield which prevents the acceleration electric field from applying the inner surface of the aperture where the secondary electrons are generated.

The Iext, Iacc and I_{H^-} as a function of the arc power are shown in Fig. 6 (a) for the grid arrangement with the shaped aperture extraction grid (the grid arrangement C). The gas pressure in the arc chamber is 3.4 mTorr. The thermal load currents, Ieg and Igg, are also shown in Fig. 6 (b), as a function of the arc power. These currents are proportional to the arc power. The power supply drain currents, Iacc and Iext, and the thermal load currents, Ieg and Igg, are apparently reduced compared with those in the grid arrangement A shown in Fig. 4, while the H^- ion current is not changed.

Figure 7 shows the I_{H^-}/Iacc and the Igg/I_{H^-} as a function of the arc power for the grid

arrangement C and D. The experimental conditions are the same as those in Fig. 6. For the grid arrangement C, the acceleration efficiency, I_{H^-}/I_{acc}, is much improved and around 85 %. The thermal load of the grounded grid is also much reduced and the I_{gg}/I_{H^-} is about 13 %, a half of that in Fig. 5. The current ratio of the I_H to the I_{ext} is about 73 % and the I_{eg}/I_{ext} is about 15 %. Thus, the leakage current of the relatively high-energy secondary electrons to the acceleration gap is suppressed. The improvement of the acceleration efficiency and the reduction of the thermal load current to the grounded grid are considered to be largely due to the decrease in the leakage of the secondary electrons generated on the inner surface of the aperture. In Fig. 7 also shown are the I_{H^-}/I_{acc} and the I_{gg}/I_{H^-} for the grid arrangement D where the same permanent magnets as those in Fig. 2 (a) are inserted in the extraction grid. The improvement of the acceleration efficiency and the reduction of the thermal load current to the grounded grid are observed by making the magnetic field strong. However, a degree of the improvement is smaller than that by shaping the aperture of the extraction grid.

C. Helium discharge

The leakage of the secondary electrons generated by the impinging of the extracted electrons to the extraction grid can be observed in helium discharge, where the only electrons are extracted. Figure 8 (a) shows the extraction current, I_{ext}, and the acceleration current, I_{acc}, as a function of the arc power in the case of the helium discharge for the grid arrangement C. Although the I_{acc} is comparable to or less than the leakage current with no load of the acceleration power supply, these currents are nearly proportional to the arc current. The current ratio of I_{acc}/I_{ext}, which indicates a degree of the secondary electron leakage, is shown in Fig. 8 (b), as a function of the arc power. The data are plotted for the grid arrangement A, C and D. It is found that the leakage of the secondary electrons to the acceleration gap is much suppressed simply by shaping the aperture of the extraction grid and that the leakage is also suppressed by strengthening the magnetic field for the electron suppression. As a result, the I_{acc}/I_{ext} is reduced to about 3 %. A degree of the improvement by making the magnetic field strong is smaller than that by shaping the extraction grid aperture. These results correspond to the improvement of the acceleration efficiency as shown in Figs. 5 and 7. Therefore, it is considered that the secondary electrons generated on the extraction grid are one of the main origins of the accelerated electrons in the grid arrangement A and B. For the grid arrangement C, the stripped electrons during the H^- ion acceleration should be the dominant origin of the accelerated electrons.

D. Stripped electron acceleration

The accelerated electrons are suppressed by shaping the extraction grid aperture. This suppression is achieved by preventing the secondary electrons generated on the extraction grid from entering the acceleration gap. The accelerated electrons also originate in the stripping loss of negative ions. Figure 9 (a) shows the I_{ext}, I_{acc} and I_{H^-} as a function of the gas pressure in the arc chamber for the grid arrangement C. The I_{eg} and I_{gg} are also shown in Fig. 9 (b). The arc power is 50 kW. The H^- ion current gradually increases with a decrease in the gas pressure down to 3 mTorr, while the thermal load current to the grounded grid, I_{gg}, monotonously decreases with a decrease in the gas pressure. The H^- ions are neutralized by the collision with the neutral gas molecules, leading to the electron detachment from the H^- ion. This stripping loss rate decreases as decreasing in the gas pressure and, therefore, the thermal load of the grounded grid also decreases as decreasing in the gas pressure.

Figure 10 shows the current ratios of I_{H^-}/I_{acc} and I_{gg}/I_{H^-} as a function of the gas pressure for the grid arrangement A and C. The data over 3 mTorr of the gas pressure are linearly fitted in the figure, since at a gas pressure below 3 mTorr the ion beam optics was not necessarily kept proper. As the gas pressure decreases, the I_{gg}/I_{H^-} decreases at nearly the same rate for both grid arrangements. However, when the gas pressure is zero, the I_{gg}/I_{H^-} for the grid arrangement C is extrapolated to about 3 %, while that for the grid arrangement A to about 15 %. This difference is ascribed to the suppression of the secondary electrons generated on the extraction grid. As shown in Fig. 10, the acceleration efficiency, I_{H^-}/I_{acc}, is also extrapolated to about 97 % at a gas pressure of 0 for the grid arrangement C. At a gas pressure of 3.4 mTorr, the I_{H^-}/I_{acc} is about 85 %, and the difference of the I_{H^-}/I_{acc} between 3.4 mTorr and 0 of the gas pressure is about 12 %, which would correspond to the stripping loss rate at a gas pressure of 3.4 mTorr. In this case, the gas pressure in the acceleration gap is estimated at 0.8 mTorr, and the calculated stripping loss rate is about 8 %. A part of the electrons generated by the negative ion stripping inside the extraction grid aperture would emerge in the acceleration gap without being trapped by the magnetic field. The backstreaming positive ions, which would increase with an increase in the gas pressure, could contribute to the acceleration drain current, I_{acc}. However, since the thermal load current to the extraction grid, I_{eg}, is almost independent of the gas pressure as shown in Fig. 9 (b), there would be no backstreaming positive ions bombarding the extraction grid. In the case of the shaped aperture extraction grid, the dominant thermal load on the grounded grid is the accelerated electrons generated by the negative ion stripping, and it is quite important to lower the operational gas pressure for the reduction of the thermal load of the grounded grid. There could be the other cause of the thermal load

corresponding to about 3 % of the negative ion current. It may be ascribed to the direct interception of the negative ions with the grounded grid.

E. Negative-ion related current loss

The plasma grid is positively biased at a few volts against the arc chamber. Figure 11 (a) shows the bias characteristics of the Iext, Iacc and I_{H^-} for the grid arrangement C. The Iext decreases monotonously with an increase in the bias voltage while the Iacc and the I_{H^-} are almost constant below 1.5 V of the bias voltage and gradually decrease over 2 V. The bias characteristics are utilized for the extracted electron suppression. The thermal load currents to the extraction and grounded grids, Ieg and Igg, are shown in Fig. 11 (b), as a function of the bias voltage for the same conditions as those in Fig. 11 (a). The Ieg decreases as the bias voltage increases while the Igg is almost constant. This implies that the extracted electrons are suppressed by the bias voltage and that the extracted electrons and the related secondary electrons do not leak to the acceleration gap. However, there is a possibility of the secondary electrons generated by the negative ion incidence to be accelerated.

Figure 12 shows the current ratios of I_{H^-}/Iacc and Igg/I_{H^-} as a function of the extraction voltage for the grid arrangement A and C. Both the extraction voltage and the acceleration voltage are changed as the ratio of the acceleration voltage to the extraction voltage is constant of 12. The arc power is 50 kW. The I_{H^-}/Iacc and the Igg/I_{H^-} are almost constant for the grid arrangement C while the I_{H^-}/Iacc and the Igg/I_{H^-} are observed to decrease and to increase, respectively, at an extraction voltage lower than 5.5 kV for the grid arrangement A. The extracted negative ion beam drifts inside the extraction grid aperture and expands due to the space-charge repulsion. At a lower extraction voltage a part of the expanding negative ion beam is incident on the inner surface of the aperture, and the secondary electrons are generated on it. In the case of the straight aperture extraction grid, these secondary electrons easily leak to the acceleration gap while they are shielded against the acceleration electric field with the narrow end aperture in the case of the shaped aperture extraction grid. Therefore, the increase in the thermal load at a lower extraction voltage is derived from the secondary electrons generated by the H^- ion bombardment for the straight aperture extraction grid. The beam optics can be kept good in a relatively wide range of the extraction voltage on the condition that the optimum voltage ratio of the acceleration to the extraction is kept.[22,24] Unless the voltage ratio is kept optimum, the thermal load of the grounded grid increases with a change of the extraction voltage due to the direct interception of the negative ion beam with the grounded grid.

The current ratios of I_{H^-}/Iacc and Igg/I_{H^-} and the FWHM of the vertical profile of the H^- ion

beam are shown in Fig. 13, as a function of the acceleration voltage for the grid arrangement C. The extraction voltage is constant of 5.6 kV and the arc power is 50 kW. The I_{H^-}/I_{acc} increases slightly and the I_{gg}/I_{H^-} decreases slightly as the acceleration voltage increases. The beamlet diameter at the grounded grid aperture would be made smaller by raising the acceleration voltage, and the direct interception of the negative ions should be reduced. However, the negative ion beamlet is over-focused and the beam divergence is larger at a higher acceleration voltage, as shown in Fig. 13. The grounded grid aperture is displaced for the multibeamlet focusing, and the maximum displacement is 3.53 mm. Therefore, the direct interception of the negative ion beam with the grounded grid is thought to be the dominant cause of the remaining thermal load at a gas pressure of 0 in Fig. 10.

IV. LONG-PULSE OPERATION

The thermal load of the extraction grid is small and the thermal load of the grounded grid is about 13 % of the negative ion beam power for the grid arrangement C. We have tested a long-pulse operation with the grid arrangement C. As a result, 330 kW of the negative ion beam (91 keV-3.6 A) was accelerated for 10 s at a gas pressure of 3.4 mTorr. The current density at the plasma grid aperture was 21 mA/cm^2 in this operation.

In conclusion, the accelerated electrons generated as the secondary electrons on the extraction grid were fully suppressed with a use of the shaped aperture extraction grid, and the thermal load of the grounded grid was much reduced. The stripped electrons generated by the negative ion neutralization are now a dominant cause of the thermal load. Lowering the operational gas pressure is only solution to the reduction of the stripped electrons. Therefore, the negative ion production efficiency is required to be improved at a lower operational gas pressure.

REFERENCES

1 Y. Okumura, M. Hanada, T. Inoue, H. Kojima, Y. Matsuda, Y. Ohara, Y. Oohara, M. Seki, Y. Suzuki and K. Watanabe, *Proc. of the 16th Symp. on Fusion Technology, London, 1990*, p. 1026.

2 Y. Takeiri, A. Ando, O. Kaneko, Y. Oka, R. Akiyama, T. Kawamoto, A. Karita, K. Mineo and T. Kuroda, *Proc. of the 16th Symp. on Fusion Technology, London, 1990*, p. 1012.

3 A. Ando, K. Tsumori, Y. Oka, O. Kaneko, Y. Takeiri, E. Asano, T. Kawamoto, R. Akiyama and T. Kuroda, Phys. Plasmas **1**, 2813 (1994).

4 Y. Takeiri, A. Ando, O. Kaneko, Y. Oka, K. Tsumori, R. Akiyama, E. Asano, T. Kawamoto, T. Kuroda, M. Tanaka and H. Kawakami, Rev. Sci. Instrum. **66**, 2541 (1995).

5 Y. Okumura, Y. Fujiwara, T. Inoue, K. Miyamoto, N. Miyamoto, A. Nagase, Y. Ohara, and K. Watanabe, Rev. Sci. Instrum. **67**, 1092 (1996).

6 A. Simonin, J. Bucalossi, C. Desgranges, M. Fumelli, C. Jacquot, P. Massmann, J. Pamela, D. Riz, and R. Trainham, Rev. Sci. Instrum. **67**, 1102 (1996).

7 R. Aymar, V. Chuyanov, M. Huguet, R. Parker, Y. Shimomura, and the ITER Joint Central Team and Home Teams, *Proc. of the 16th IAEA Fusion Energy Conference, Montreal, Canada, 1996*, IAEA-CN-64/O1-1.

8 R. S. Hemsworth, J.-H. Feist, M. Hanada, B. Heinemann, T. Inoue, E. Kussel, A. Krylov, P. Lotte, K. Miyamoto, N. Miyamoto, D. Murdoch, A. Nagase, Y. Ohara, Y. Okumura, J. Pamela, A. Panasenkov, K. Shibata, M. Tanii, and M. Watson, Rev. Sci. Instrum. **67**, 1120 (1996).

9 K. Miyamoto, N. Akino, T. Aoyagi, N. Ebisawa, Y. Fujiwara, A. Honda, T. Inoue, T. Itoh, M. Kawai, M. Kazawa, J. Koizumi, M. Kuriyama, N. Miyamoto, K. Mogaki, Y. Ohara, T. Ohga, K. Ohshima, Y. Okumura, H. Oohara, F. Satoh, K. Usui, K. Watanabe, M. Yamamoto, T. Yamazaki, *Proc. of the 16th IAEA Fusion Energy Conference, Montreal, Canada, 1996*, IAEA-CN-64/GP-10.

10 K. Ushigusa and The JT-60 Team, *Proc. of the 16th IAEA Fusion Energy Conference, Montreal, Canada, 1996*, IAEA-CN-64/O1-3.

11 P. Massmann, J. Bucalossi, D. Ciric, C. Desgranges, M. Fumelli, J. Pamela, and A. Simonin, *Proc. of the 16th IAEA Fusion Energy Conference, Montreal, Canada, 1996*, IAEA-CN-64/GP-13.

12 A. Ando, Y. Takeiri, K. Tsumori, O. Kaneko, Y. Oka, R. Akiyama, T. Kawamoto, K. Mineo, T. Kurata and T. Kuroda, Rev. Sci. Instrum. **63**, 2683 (1992).

13 O. Kaneko, A. Ando, Y. Oka, Y. Takeiri, K. Tsumori, R. Akiyama, T. Kawamoto, T.

Kurata, K. Mineo and T. Kuroda, *Proc. of the 17th Symp.on Fusion Technology, Rome, 1992*, p. 544.

14 A. Ando, K. Tsumori, Y. Takeiri, O. Kaneko, Y. Oka, T. Okumura, H. Kojima, Y. Yamashita, R. Akiyama, T. Kawamoto, K. Mineo, T. Kurata and T. Kuroda, *Proc. of the 6th Int. Symp. on Production and Neutralization of Negative Ions and Beams, Upton, NY, 1992*, AIP Conf. Proc. No. 287, p. 339.

15 Y. Takeiri, A. Ando, O. Kaneko, Y. Oka, K. Tsumori, R. Akiyama, T. Kawamoto and T. Kuroda, *Proc. of the 6th Int. Symp. on Production and Neutralization of Negative Ions and Beams, Upton, NY, 1992*, AIP Conf. Proc. No. 287, p. 869.

16 Y. Oka, Y. Takeiri, O. Kaneko, A. Ando, K. Tsumori, R. Akiyama, T. Kawamoto, and T. Kuroda, Rev. Sci. Instrum. **65**, 1192 (1994).

17 K. Tsumori, A. Ando, Y. Takeiri, O. Kaneko, Y. Oka, T. Okuyama, H. Kojima, Y. Yamashita, T. Kawamoto, R. Akiyama and T. Kuroda, Rev. Sci. Instrum. **65**, 1195 (1994).

18 Y. Takeiri, Y. Oka, O. Kaneko, A. Ando, K. Tsumori, R. Akiyama, T. Kawamoto, and T. Kuroda, Rev. Sci. Instrum. **65**, 1198 (1994).

19 K. Tsumori, A. Ando, T. Okuyama, Y. Suzuki, O. Kaneko, Y. Oka, Y. Takeiri, R. Akiyama, T. Kawamoto, K. Seko, and T. Kuroda, Fusion Engineering and Design **26**, 473 (1995).

20 Y. Takeiri, A. Ando, O. Kaneko, Y. Oka, K. Tsumori, T. Takanashi, R. Akiyama, E. Asano, T. Kawamoto, M. Tanaka, H. Kawakami, T. Okuyama, Y. Suzuki and T. Kuroda, *Proc. of the 18th Symposium on Fusion Technology, Karlsruher, 1994*, Vol. 1, North-Holland, Amsterdam (1995) p. 609.

21 Y. Takeiri, A. Ando, O. Kaneko, Y. Oka, K. Tsumori, R. Akiyama, E. Asano, T. Kawamoto, M. Tanaka and T. Kuroda, J. Plasma Fusion Res. **71**, 605 (1995).

22 Y. Takeiri, O. Kaneko, Y. Oka, K. Tsumori, E. Asano, R. Akiyama, T. Kawamoto, T. Kuroda, and A. Ando, Rev. Sci. Instrum. **66**, 5236 (1995).

23 Y. Takeiri, O. Kaneko, Y. Oka, K. Tsumori, E. Asano, R. Akiyama, T. Kawamoto, T. Kuroda, and A. Ando, Rev. Sci. Instrum. **67**, 1021 (1996).

24 A. Ando, Y. Takeiri, O. Kaneko, Y. Oka, K. Tsumori, E. Asano, T. Kawamoto, R. Akiyama, and T. Kuroda, Rev. Sci. Instrum. **66**, 5412 (1995).

25 Y. Takeiri, O. Kaneko, F. Sano, A. Ando, Y. Oka, K. Hanatani, T. Obiki and T. Kuroda, *Proc. of the first Int. Toki Conf. on Plasma Physics and Controlled Nuclear Fusion, Toki, Japan, 1989*, p. 272.

26 O. Kaneko, Y. Takeiri, K. Tsumori, Y. Oka, M. Osakabe, R. Akiyama, T. Kawamoto, E.

Asano, and T. Kuroda, *Proc. of the 16th IAEA Fusion Energy Conference, Montreal, Canada, 1996*, IAEA-CN-64/GP-9.

27 A. Iiyoshi, M. Fujiwara, O. Motojima, N. Ohyabu and K. Yamazaki, Fusion Technology **17**, 169 (1990).

28 S. R. Walther, K. N. Leung and W. B. Kunkel, J. Appl. Phys. **64**, 3424 (1988).

29 K. N. Leung, C. A. Hauck, W. B. Kunkel and S. R. Walther, Rev. Sci. Instrum. **60**, 531 (1989).

30 Y. Okumura, M. Hanada, T. Inoue, M. Mizuno, Y. Ohara, Y. Suzuki, H. Tanaka, M. Tanaka, and K. Watanabe, Rev. Sci. Instrum. **63**, 2708 (1992).

31 M. Mizuno, M. Hanada, T. Inoue, S. Maeno, Y. Ohara, Y. Okumura, M. Tanaka, and K. Watanabe, *Proc. of the 6th Int. Symp. on Production and Neutralization of Negative Ions and Beams, Upton, NY, 1992*, AIP Conf. Proc. No. 287, p. 710.

32 K. Miyamoto, M. Hanada, T. Inoue, N. Miyamoto, A. Nagase, Y. Ohara, Y. Okumura, K. Watanabe, *Proc. of the 18th Symposium on Fusion Technology, Karlsruher, 1994*, Vol. 1, North-Holland, Amsterdam (1995) p. 625.

FIGURE CAPTIONS

Fig. 1 Schematic diagram of an external filter type large hydrogen negative ion source.

Fig. 2 Grid arrangements (a) with a straight aperture extraction grid (grid arrangement B) and (b) with a shaped aperture extraction grid (grid arrangement C). Grid arrangement without the electron suppression grid in (a) is the grid arrangement A, and in (b) grid arrangement using the same permanent magnets as those in (a) is the grid arrangement D.

Fig. 3 Example of the time evolution of the water temperature rise of the grounded grid and the extraction grid. The beam pulse length is 0.6 s.

Fig. 4 (a) Extraction current, I_{ext}, the acceleration current, I_{acc}, the H^- ion current, I_{H^-}, and the acceleration voltage, V_{acc}, and (b) the equivalent thermal load currents to the extraction grid, I_{eg}, and to the grounded grid, I_{gg}, as a function of the arc power for the grid arrangement A. The gas pressure in the arc chamber is 3.2 mTorr.

Fig. 5 Ratio of the H^- ion current to the acceleration drain current, I_{H^-}/I_{acc}, and the ratio of the equivalent thermal load current to the grounded grid to the H^- ion current, I_{gg}/I_{H^-}, as a function of the arc power for the grid arrangement A and B. The gas pressure in the arc chamber is 3.2 mTorr.

Fig. 6 (a) Extraction current, I_{ext}, the acceleration current, I_{acc}, and the H^- ion current, I_{H^-}, and (b) the equivalent thermal load currents to the extraction grid, I_{eg}, and to the grounded grid, I_{gg}, as a function of the arc power for the grid arrangement C. The gas pressure in the arc chamber is 3.4 mTorr.

Fig. 7 Ratio of the H^- ion current to the acceleration drain current, I_{H^-}/I_{acc}, and the ratio of the equivalent thermal load current to the grounded grid to the H^- ion current, I_{gg}/I_{H^-}, as a function of the arc power for the grid arrangement C and D. The gas pressure in the arc chamber is 3.4 mTorr.

Fig. 8 (a) Extraction current, I_{ext}, and the acceleration current, I_{acc}, for the grid arrangement C, and (b) the current ratio of the acceleration to the extraction, I_{acc}/I_{ext}, for the grid arrangement A, C and D, as a function of the arc power in the case of the helium discharge.

Fig. 9 (a) Extraction current, I_{ext}, the acceleration current, I_{acc}, and the H^- ion current, I_{H^-}, and (b) the equivalent thermal load currents to the extraction grid, I_{eg}, and to the grounded grid, I_{gg}, for the grid arrangement C, as a function of the gas pressure in the arc chamber. The arc power is 50 kW.

Fig. 10 Ratio of the H^- ion current to the acceleration drain current, I_{H^-}/I_{acc}, and the ratio of the

equivalent thermal load current to the grounded grid to the H^- ion current, I_{gg}/I_{H^-}, for the grid arrangement A and C. as a function of the gas pressure in the arc chamber. The arc power is 50 kW. The data are linearly fitted by solid lines over 3 mTorr of the gas pressure.

Fig. 11 (a) Extraction current, I_{ext}, the acceleration current, I_{acc}, and the H^- ion current, I_{H^-}, and (b) the equivalent thermal load currents to the extraction grid, I_{eg}, and to the grounded grid, I_{gg}, as a function of the bias voltage for the grid arrangement C. The arc power is 50 kW and the gas pressure in the arc chamber is 3.4 mTorr.

Fig. 12 Ratio of the H^- ion current to the acceleration drain current, I_{H^-}/I_{acc}, and the ratio of the equivalent thermal load current to the grounded grid to the H^- ion current, I_{gg}/I_{H^-}, as a function of the extraction voltage for the grid arrangement A and C. The ratio of the acceleration voltage to the extraction voltage is constant of 12. The arc power is 50 kW.

Fig. 13 Ratio of the H^- ion current to the acceleration drain current, I_{H^-}/I_{acc}, the ratio of the equivalent thermal load current to the grounded grid to the H^- ion current, I_{gg}/I_{H^-}, and the FWHM of the vertical profile of the H^- ion beam as a function of the acceleration voltage for the grid arrangement C. The extraction voltage is constant of 5.6 kV. The arc power is 50 kW and the gas pressure in the arc chamber is 3.4 mTorr.

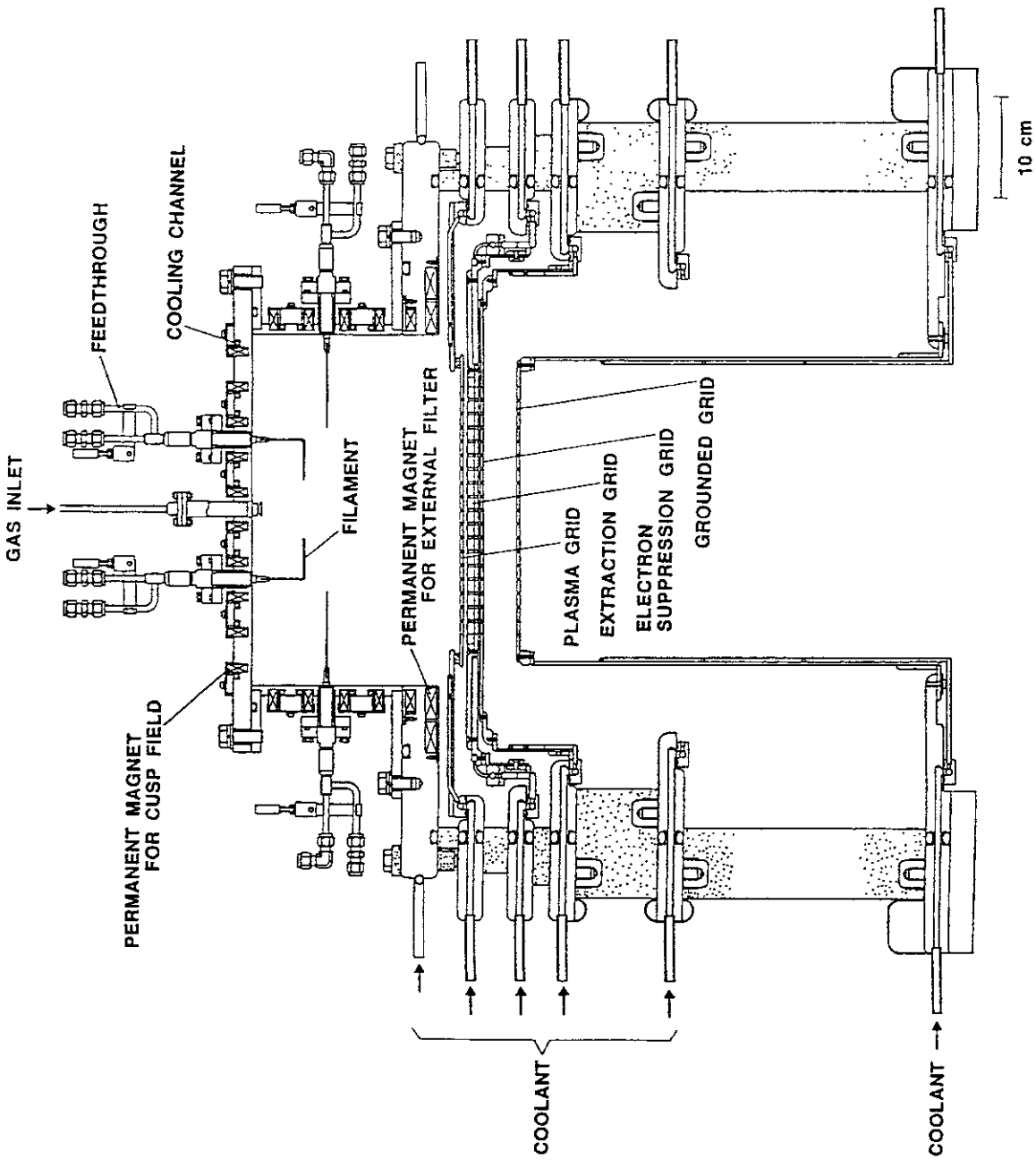

Figure 1
Y. Takeiri, *et al.*

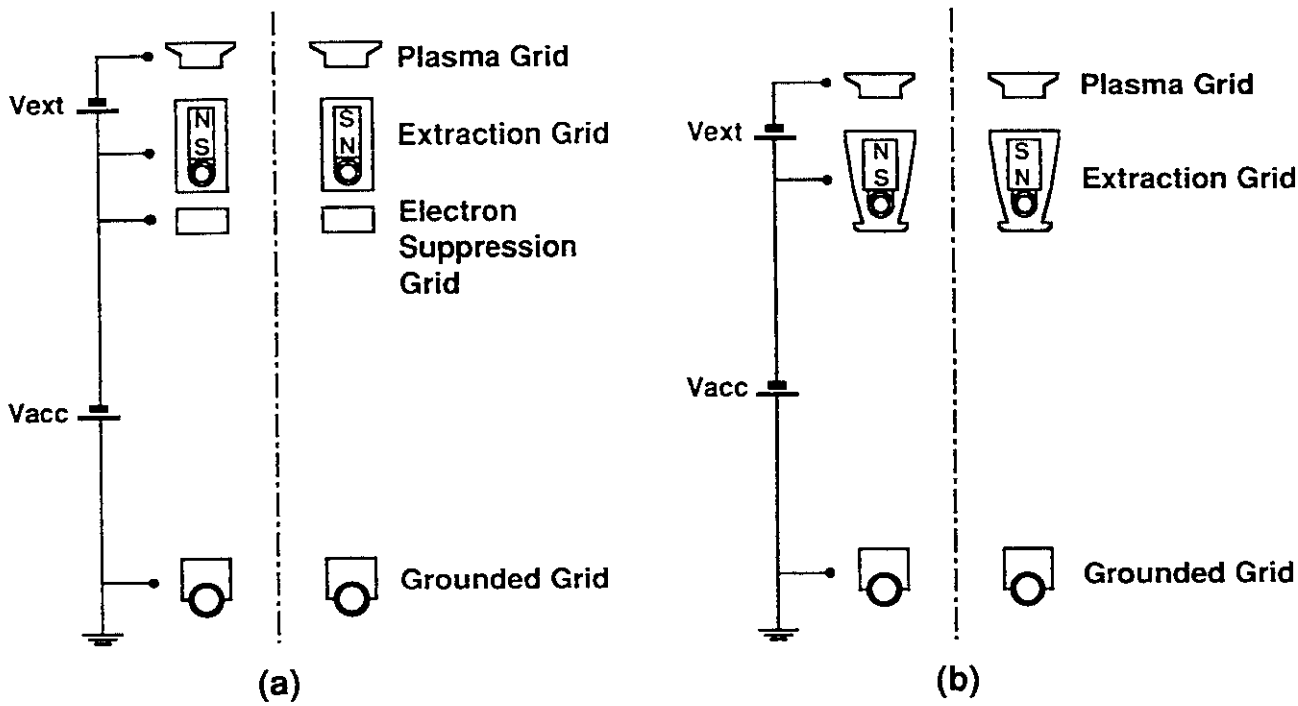

Figure 2
Y. Takeiri, *et al.*

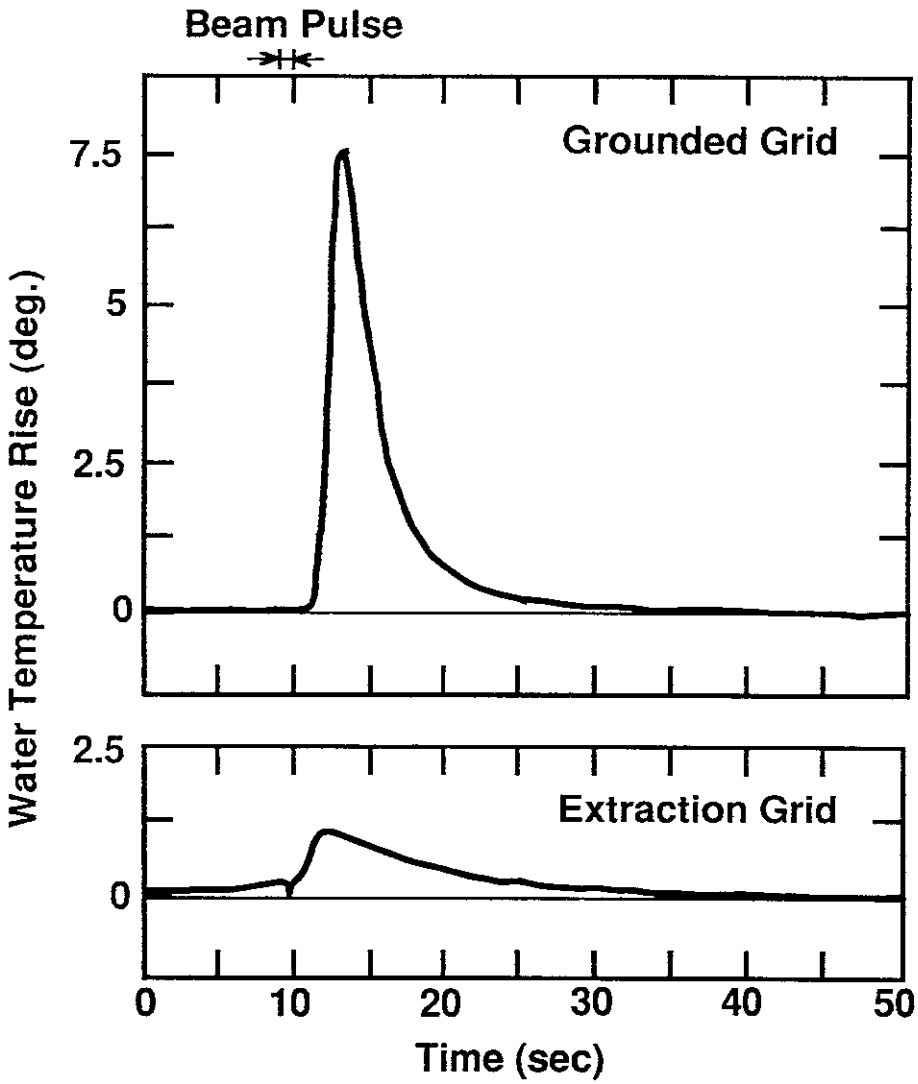

Figure 3
Y. Takeiri, *et al.*

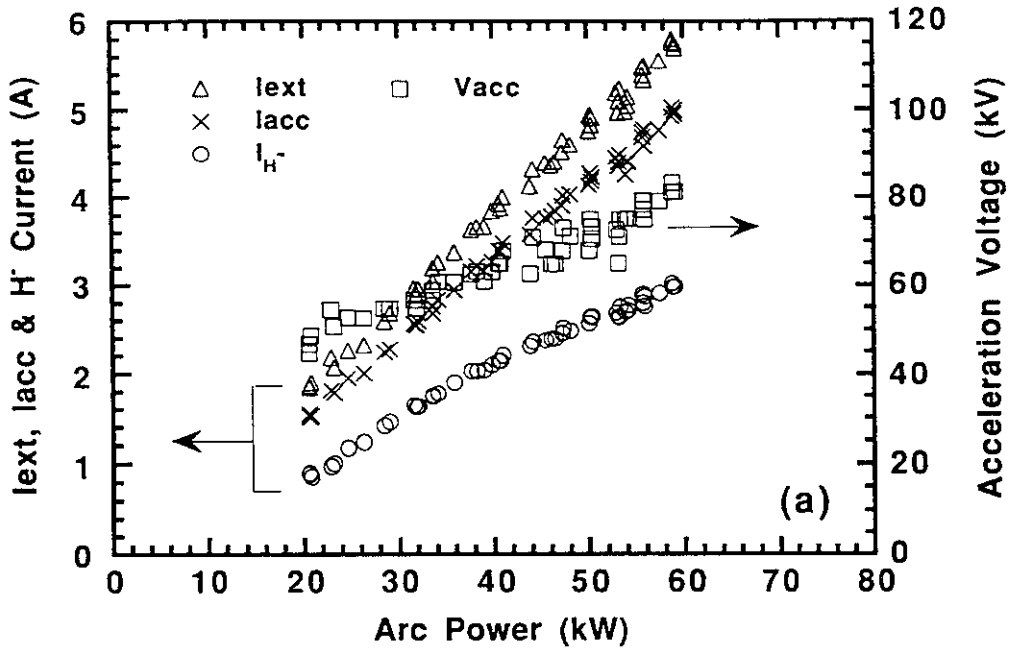

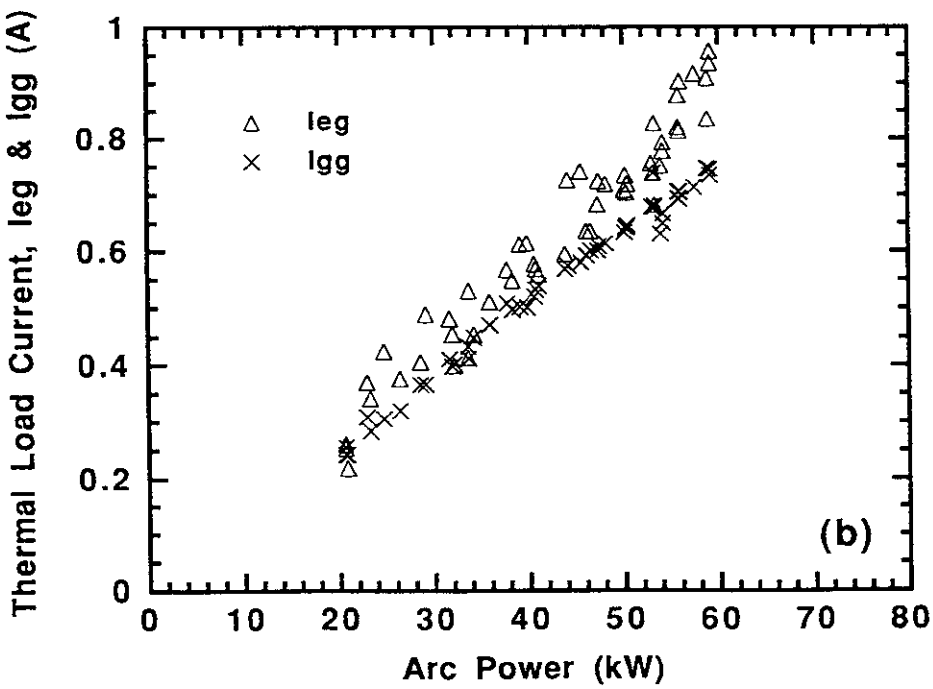

Figure 4
Y. Takeiri, *et al.*

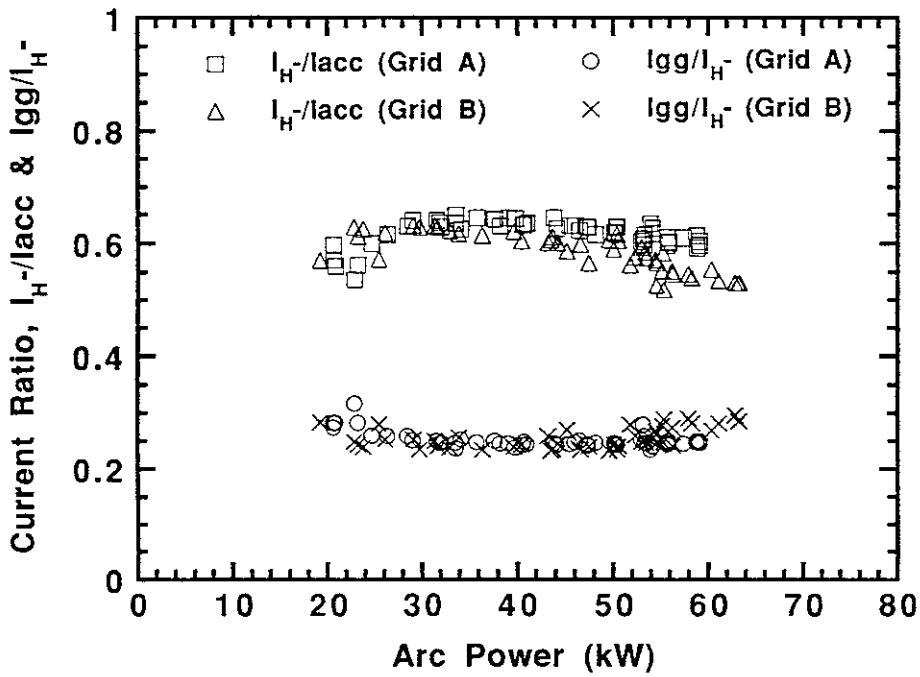

Figure 5
Y. Takeiri, *et al.*

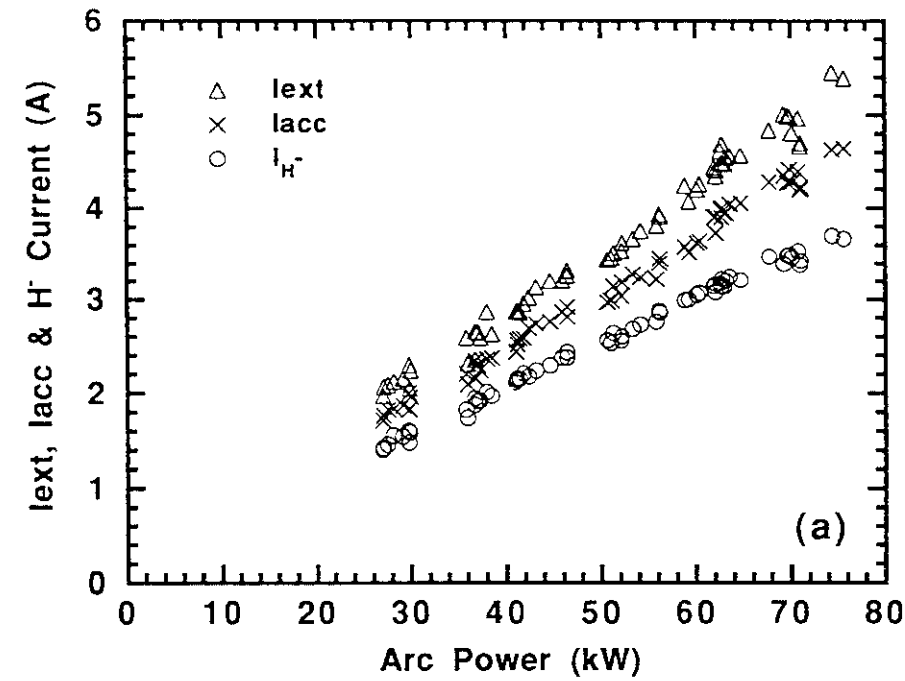

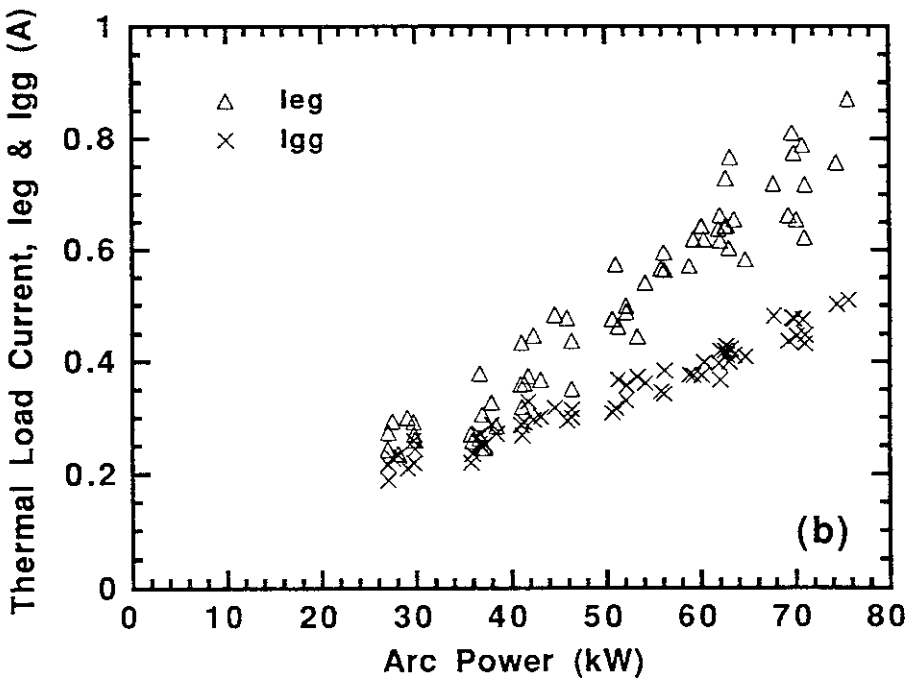

Figure 6
Y. Takeiri, *et al.*

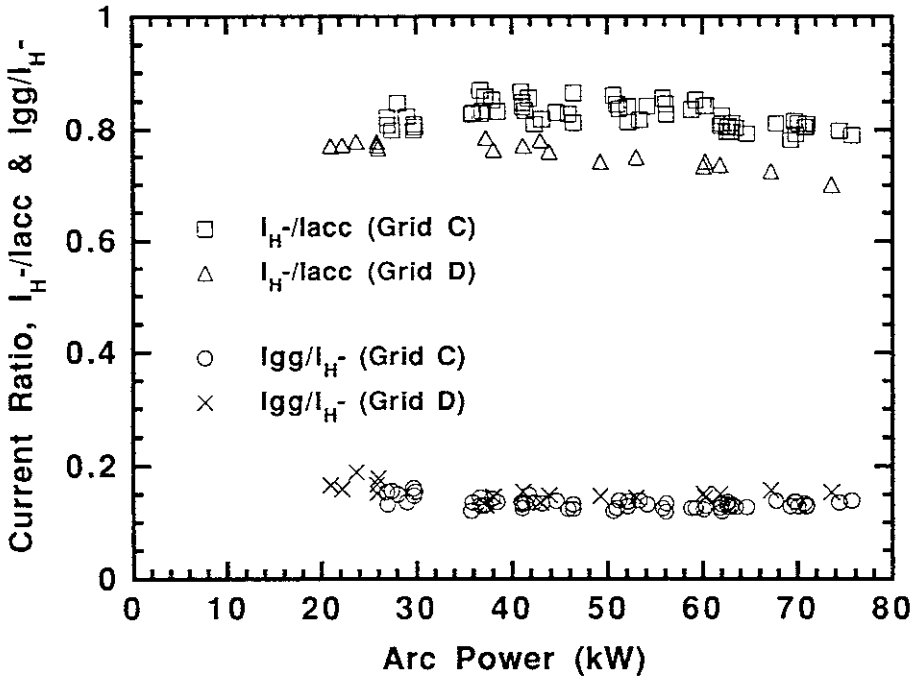

Figure 7
Y. Takeiri, *et al.*

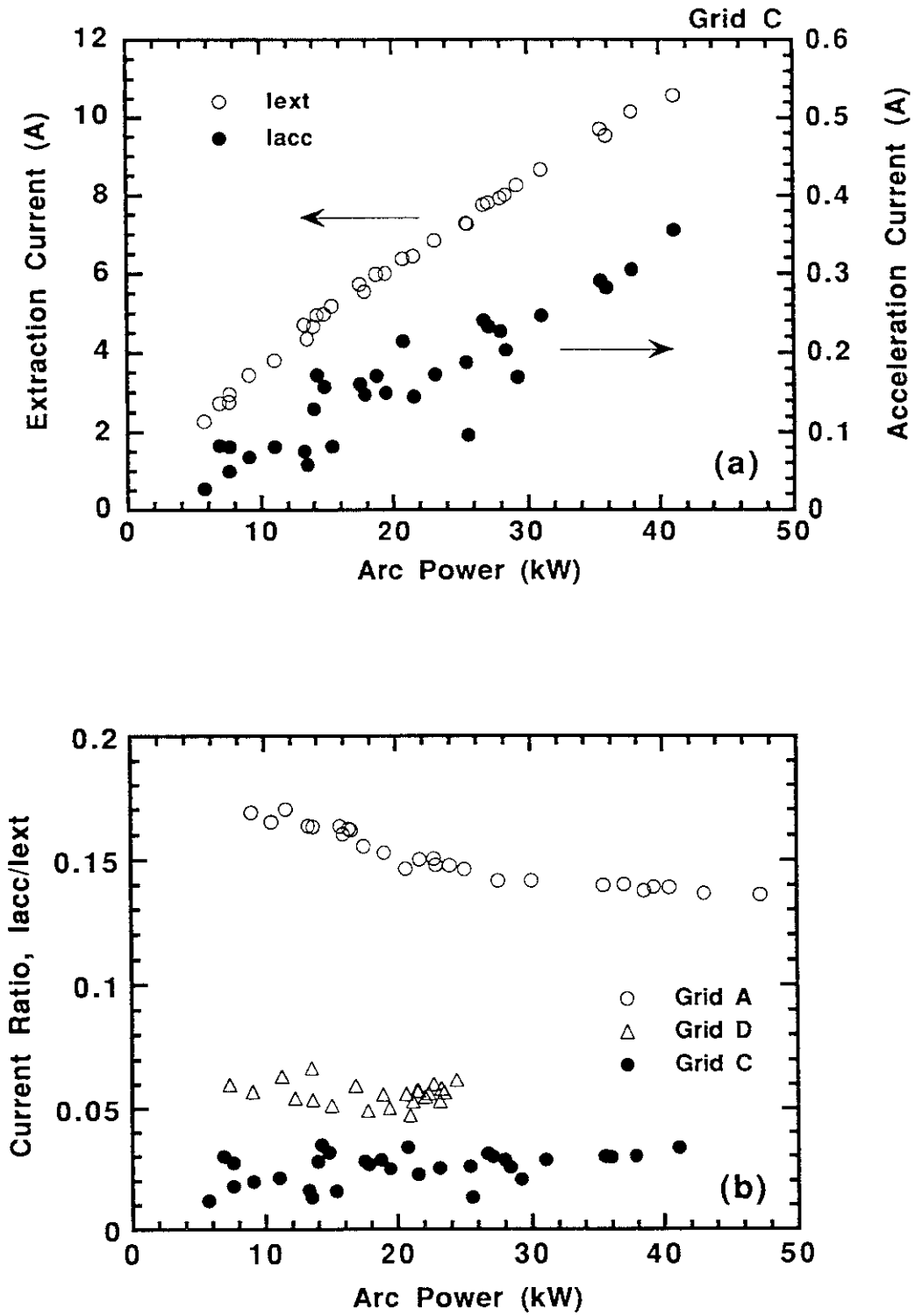

Figure 8
Y. Takeiri, *et al.*

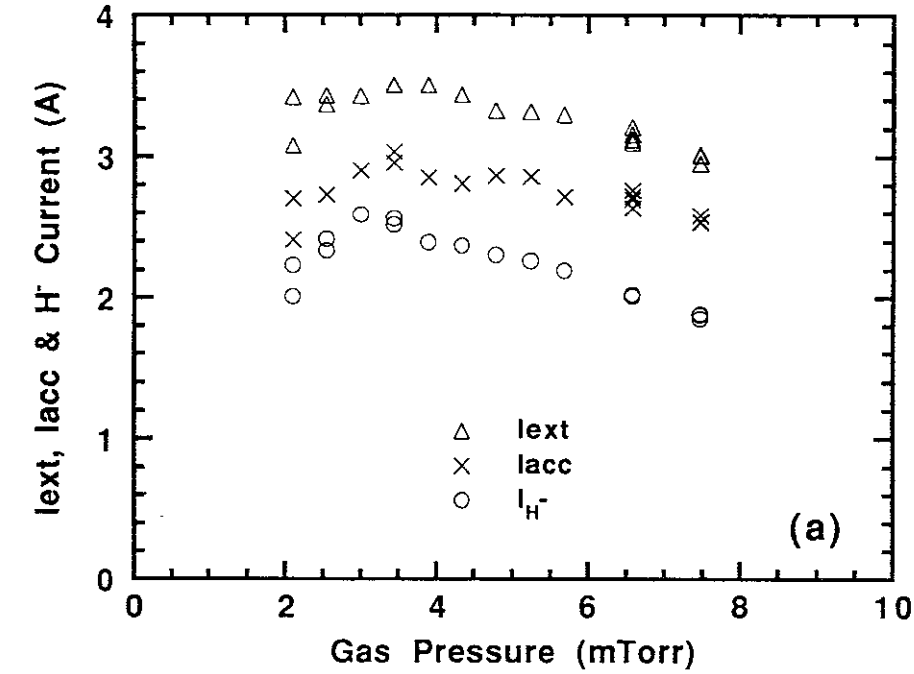

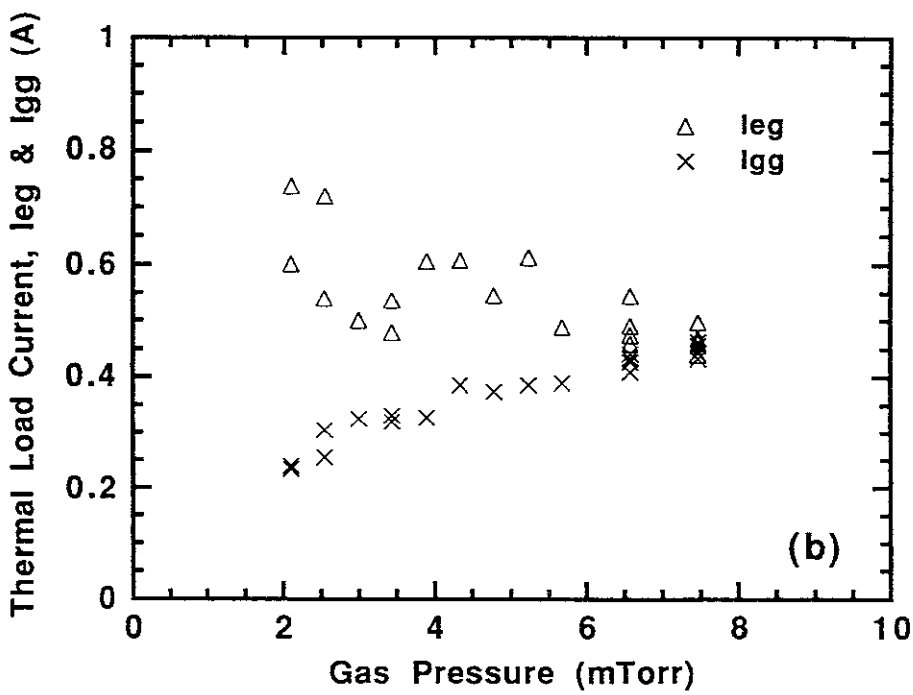

Figure 9
Y. Takeiri, *et al.*

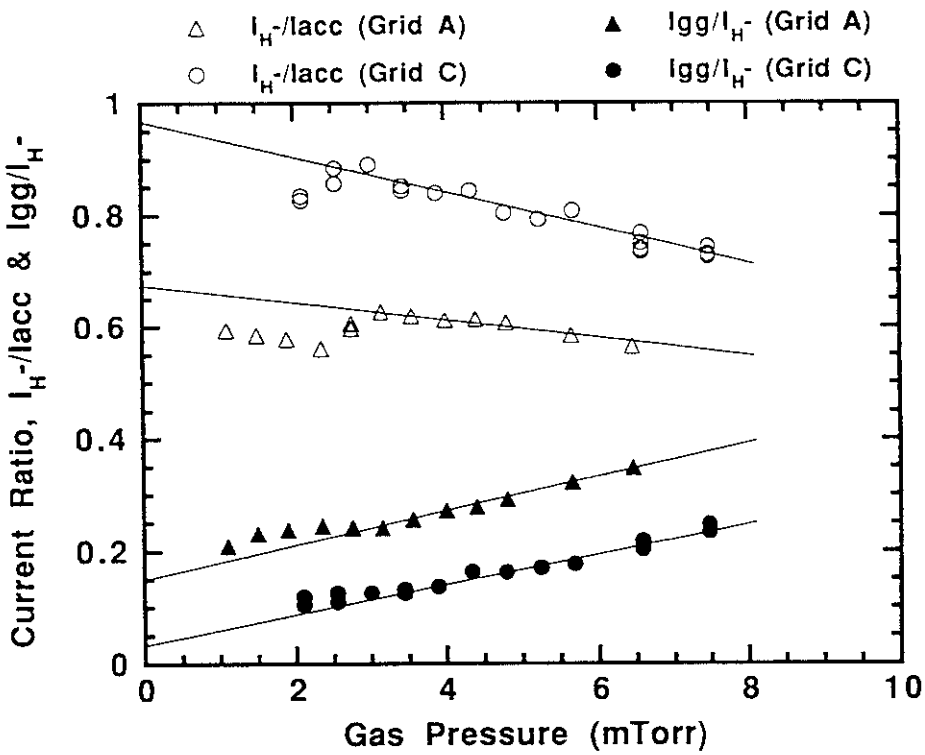

Figure 10
Y. Takeiri, *et al.*

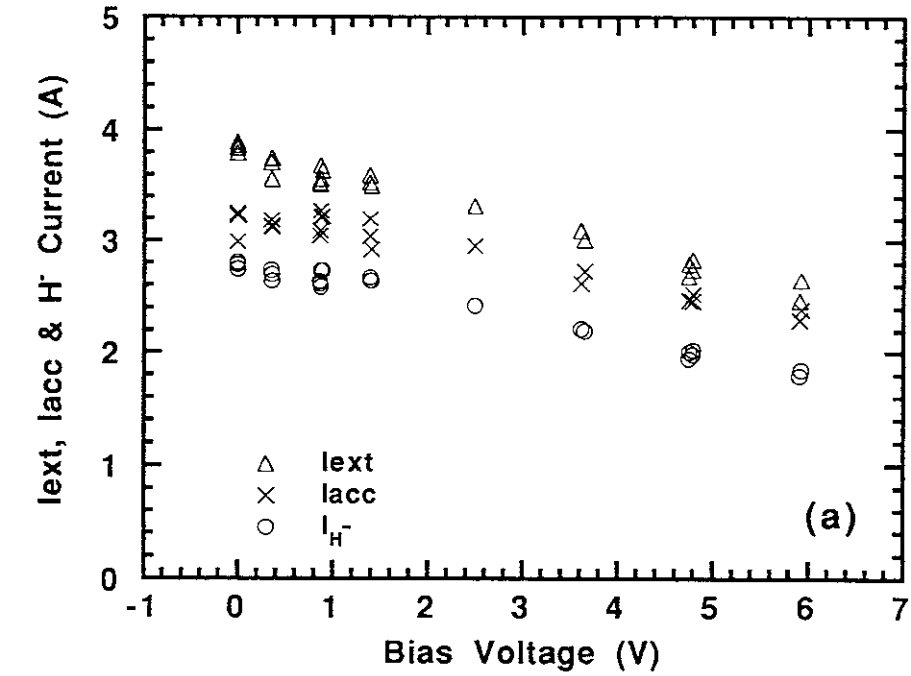

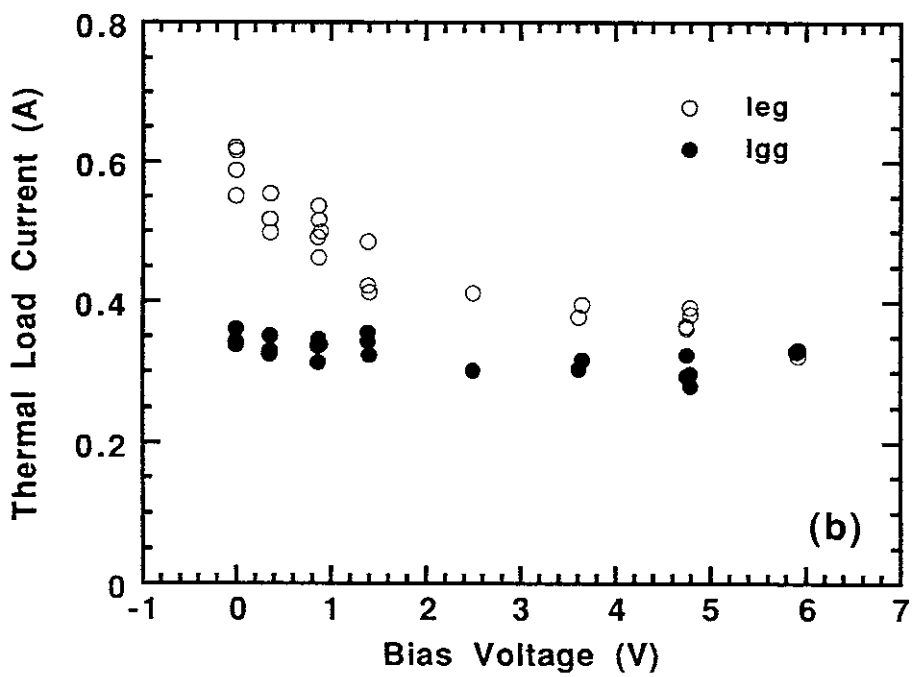

Figure 11
Y. Takeiri, *et al.*

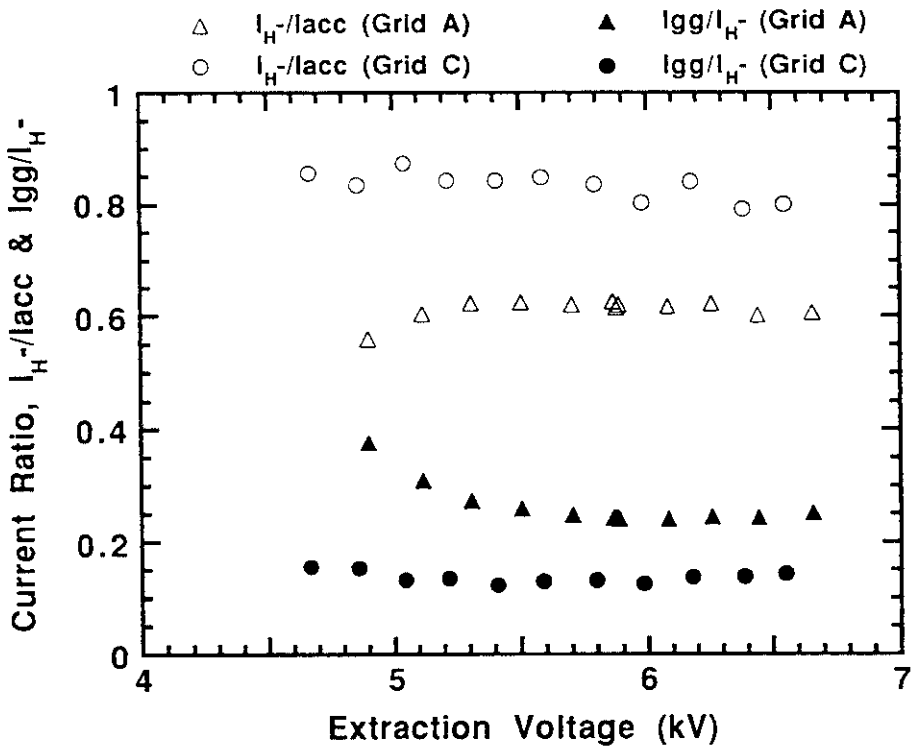

Figure 12
Y. Takeiri, *et al.*

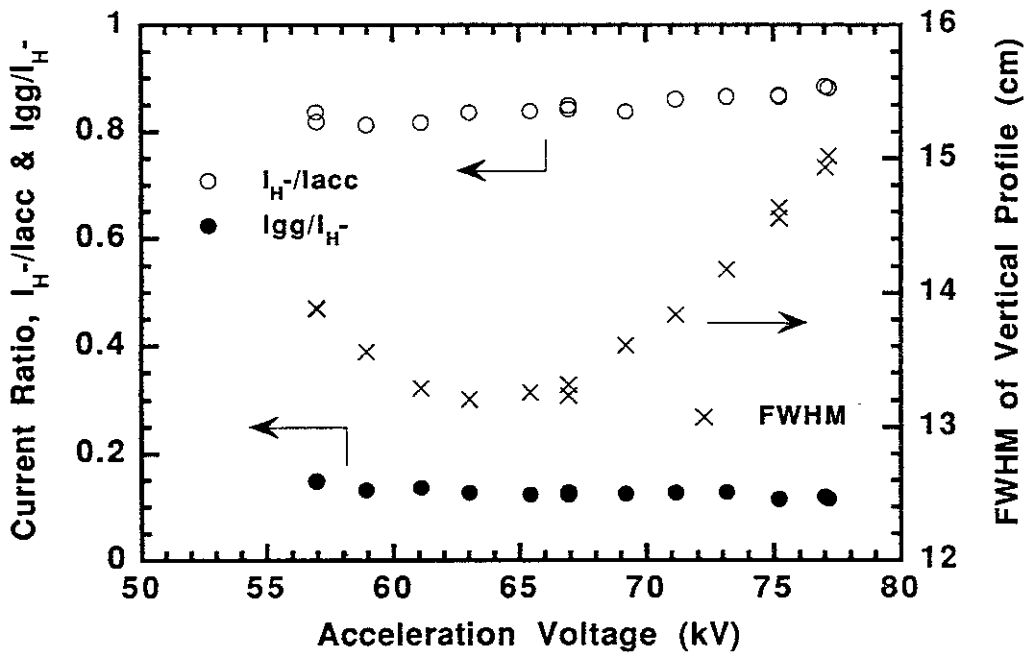

Figure 13
Y. Takeiri, *et al.*

Recent Issues of NIFS Series

NIFS-428 V.Yu. Sergeev, K.V. Khlopenkov, B.V Kuteev, S. Sudo, K. Kondo, F. Sano, H. Zushi, H. Okada, S. Besshou, T. Mizuuchi, K. Nagasaki, Y. Kurimoto and T. Obiki,
Recent Experiments on Li Pellet Injection into Heliotron E; Aug. 1996

NIFS-429 N. Noda, V. Philipps and R. Neu,
A Review of Recent Experiments on W and High Z Materials as Plasma-Facing Components in Magnetic Fusion Devices; Aug. 1996

NIFS-430 R.L. Tobler, A. Nishimura and J. Yamamoto,
Design-Relevant Mechanical Properties of 316-Type Stainless Steels for Superconducting Magnets; Aug. 1996

NIFS-431 K. Tsuzuki, M. Natsir, N. Inoue, A. Sagara, N. Noda, O. Motojima, T. Mochizuki, T. Hino and T. Yamashina,
Hydrogen Absorption Behavior into Boron Films by Glow Discharges in Hydrogen and Helium; Aug. 1996

NIFS-432 T.-H. Watanabe, T. Sato and T. Hayashi,
Magnetohydrodynamic Simulation on Co- and Counter-helicity Merging of Spheromaks and Driven Magnetic Reconnection; Aug. 1996

NIFS-433 R. Horiuchi and T. Sato,
Particle Simulation Study of Collisionless Driven Reconnection in a Sheared Magnetic Field; Aug. 1996

NIFS-434 Y. Suzuki, K. Kusano and K. Nishikawa,
Three-Dimensional Simulation Study of the Magnetohydrodynamic Relaxation Process in the Solar Corona. II.; Aug. 1996

NIFS-435 H. Sugama and W. Horton,
Transport Processes and Entropy Production in Toroidally Rotating Plasmas with Electrostatic Turbulence; Aug. 1996

NIFS-436 T. Kato, E. Rachlew-Källne, P. Hörling and K.-D Zastrow,
Observations and Modelling of Line Intensity Ratios of OV Multiplet Lines for 2s3s 3S1 - 2s3p 3Pj; Aug. 1996

NIFS-437 T. Morisaki, A. Komori, R. Akiyama, H. Idei, H. Iguchi, N. Inoue, Y. Kawai, S. Kubo, S. Masuzaki, K. Matsuoka, T. Minami, S. Morita, N. Noda, N. Ohyabu, S. Okamura, M. Osakabe, H. Suzuki, K. Tanaka, C. Takahashi, H. Yamada, I. Yamada and O. Motojima,
Experimental Study of Edge Plasma Structure in Various Discharges on Compact Helical System; Aug. 1996

NIFS-438 A. Komori, N. Ohyabu, S. Masuzaki, T. Morisaki, H. Suzuki, C. Takahashi, S. Sakakibara, K. Watanabe, T. Watanabe, T. Minami, S. Morita, K. Tanaka, S.

Ohdachi, S. Kubo, N. Inoue, H. Yamada, K. Nishimura. S. Okamura, K. Matsuoka, O. Motojima, M. Fujiwara, A. Iiyoshi, C. C. Klepper, J.F. Lyon, A.C. England, D.E. Greenwood, D.K. Lee, D.R. Overbey, J.A. Rome, D.E. Schechter and C.T. Wilson,
Edge Plasma Control by a Local Island Divertor in the Compact Helical System; Sep. 1996 (IAEA-CN-64/C1-2)

NIFS-439 K. Ida, K. Kondo, K. Nagaski T. Hamada, H. Zushi, S. Hidekuma, F. Sano, T. Mizuuchi, H. Okada, S. Besshou, H. Funaba, Y. Kurimoto, K. Watanabe and T. Obiki,
Dynamics of Ion Temperature in Heliotron-E; Sep. 1996 (IAEA-CN-64/CP-5)

NIFS-440 S. Morita, H. Idei, H. Iguchi, S. Kubo, K. Matsuoka, T. Minami, S. Okamura, T. Ozaki, K. Tanaka, K. Toi, R. Akiyama, A. Ejiri, A. Fujisawa, M. Fujiwara, M. Goto, K. Ida, N. Inoue, A. Komori, R. Kumazawa, S. Masuzaki, T. Morisaki, S. Muto, K. Narihara, K. Nishimura, I. Nomura, S. Ohdachi, M.. Osakabe, A. Sagara, Y. Shirai, H. Suzuki, C. Takahashi, K. Tsumori, T. Watari, H. Yamada and I. Yamada,
A Study on Density Profile and Density Limit of NBI Plasmas in CHS; Sep. 1996 (IAEA-CN-64/CP-3)

NIFS-441 O. Kaneko, Y. Takeiri, K. Tsumori, Y. Oka, M. Osakabe, R. Akiyama, T. Kawamoto, E. Asano and T. Kuroda,
Development of Negative-Ion-Based Neutral Beam Injector for the Large Helical Device; Sep. 1996 (IAEA-CN-64/GP-9)

NIFS-442 K. Toi, K.N. Sato, Y. Hamada, S. Ohdachi, H. Sakakita, A. Nishizawa, A. Ejiri, K. Narihara, H. Kuramoto, Y. Kawasumi, S. Kubo, T. Seki, K. Kitachi, J. Xu, K. Ida, K. Kawahata, I. Nomura, K. Adachi, R. Akiyama, A. Fujisawa, J. Fujita, N. Hiraki, S. Hidekuma, S. Hirokura, H. Idei, T. Ido, H. Iguchi, K. Iwasaki, M. Isobe, O. Kaneko, Y. Kano, M. Kojima, J. Koog, R. Kumazawa, T. Kuroda, J. Li, R. Liang, T. Minami, S. Morita, K. Ohkubo, Y. Oka, S. Okajima, M. Osakabe, Y. Sakawa, M. Sasao, K. Sato, T. Shimpo, T. Shoji, H. Sugai, T. Watari, I. Yamada and K. Yamauti,
Studies of Perturbative Plasma Transport, Ice Pellet Ablation and Sawtooth Phenomena in the JIPP T-IIU Tokamak; Sep. 1996 (IAEA-CN-64/A6-5)

NIFS-443 Y. Todo, T. Sato and The Complexity Simulation Group,
Vlasov-MHD and Particle-MHD Simulations of the Toroidal Alfvén Eigenmode; Sep. 1996 (IAEA-CN-64/D2-3)

NIFS-444 A. Fujisawa, S. Kubo, H. Iguchi, H. Idei, T. Minami, H. Sanuki, K. Itoh, S. Okamura, K. Matsuoka, K. Tanaka, S. Lee, M. Kojima, T.P. Crowley, Y. Hamada, M. Iwase, H. Nagasaki, H. Suzuki, N. Inoue, R. Akiyama, M. Osakabe, S. Morita, C. Takahashi, S. Muto, A. Ejiri, K. Ida, S. Nishimura, K. Narihara, I. Yamada, K. Toi, S. Ohdachi, T. Ozaki, A. Komori, K. Nishimura, S. Hidekuma, K. Ohkubo, D.A. Rasmussen, J.B. Wilgen, M. Murakami, T. Watari and M. Fujiwara,
An Experimental Study of Plasma Confinement and Heating Efficiency through the Potential Profile Measurements with a Heavy Ion Beam Probe

in the Compact Helical System; Sep. 1996 (IAEA-CN-64/C1-5)

NIFS-445 O. Motojima, N. Yanagi, S. Imagawa, K. Takahata, S. Yamada, A Iwamoto, H. Chikaraishi, S. Kitagawa, R. Maekawa, S. Masuzaki, T. Mito, T. Morisaki, A. Nishimura, S. Sakakibara, S. Satoh, T. Satow, H. Tamura, S. Tanahashi, K. Watanabe, S. Yamaguchi, J. Yamamoto, M.Fujiwara and A. Iiyoshi,
Superconducting Magnet Design and Construction of LHD, Sep. 1996 (IAEA-CN-64/G2-4)

NIFS-446 S. Murakami, N. Nakajima, S. Okamura, M. Okamoto and U. Gasparino,
Orbit Effects of Energetic Particles on the Reachable β–Value and the Radial Electric Field in NBI and ECR Heated Heliotron Plasmas; Sep. 1996 (IAEA-CN-64/CP -6) Sep. 1996

NIFS-447 K. Yamazaki, A. Sagara, O. Motojima, M. Fujiwara, T. Amano, H. Chikaraishi, S. Imagawa, T. Muroga, N. Noda, N. Ohyabu, T. Satow, J.F. Wang, K.Y. Watanabe, J. Yamamoto . H. Yamanishi, A. Kohyama, H. Matsui, O. Mitarai, T. Noda, A.A. Shishkin, S. Tanaka and T. Terai
Design Assessment of Heliotron Reactor; Sep. 1996 (IAEA-CN-64/G1-5)

NIFS-448 M. Ozaki, T. Sato and the Complexity Simulation Group,
Interactions of Convecting Magnetic Loops and Arcades; Sep. 1996

NIFS-449 T. Aoki,
Interpolated Differential Operator (IDO) Scheme for Solving Partial Differential Equations; Sep. 1996

NIFS-450 D. Biskamp and T. Sato,
Partial Reconnection in the Sawtooth Collapse; Sep. 1996

NIFS-451 J. Li, X. Gong, L. Luo, F.X. Yin, N. Noda, B. Wan, W. Xu, X. Gao, F. Yin, J.G. Jiang, Z. Wu., J.Y. Zhao, M. Wu, S. Liu and Y. Han,
Effects of High Z Probe on Plasma Behavior in HT-6M Tokamak; Sep. 1996

NIFS-452 N. Nakajima, K. Ichiguchi, M. Okamoto and R.L. Dewar,
Ballooning Modes in Heliotrons/Torsatrons; Sep. 1996 (IAEA-CN-64/D3-6)

NIFS-453 A. Iiyoshi,
Overview of Helical Systems; Sep. 1996 (IAEA-CN-64/O1-7)

NIFS-454 S. Saito, Y. Nomura, K. Hirose and Y.H. Ichikawa,
Separatrix Reconnection and Periodic Orbit Annihilation in the Harper Map; Oct. 1996

NIFS-455 K. Ichiguchi, N. Nakajima and M. Okamoto,
Topics on MHD Equilibrium and Stability in Heliotron / Torsatron; Oct. 1996

NIFS-456 G. Kawahara, S. Kida, M. Tanaka and S. Yanase,

Wrap, Tilt and Stretch of Vorticity Lines around a Strong Straight Vortex Tube in a Simple Shear Flow; Oct. 1996

NIFS-457 K. Itoh, S.- I. Itoh, A. Fukuyama and M. Yagi,
Turbulent Transport and Structural Transition in Confined Plasmas; Oct. 1996

NIFS-458 A. Kageyama and T. Sato,
Generation Mechanism of a Dipole Field by a Magnetohydrodynamic Dynamo; Oct. 1996

NIFS-459 K. Araki, J. Mizushima and S. Yanase,
The Non-axisymmetric Instability of the Wide-Gap Spherical Couette Flow; Oct. 1996

NIFS-460 Y. Hamada, A. Fujisawa, H. Iguchi, A. Nishizawa and Y. Kawasumi,
A Tandem Parallel Plate Analyzer; Nov. 1996

NIFS-461 Y. Hamada, A. Nishizawa, Y. Kawasumi, A. Fujisawa, K. Narihara, K. Ida, A. Ejiri, S. Ohdachi, K. Kawahata, K. Toi, K. Sato, T. Seki, H. Iguchi, K. Adachi, S. Hidekuma, S.Hirokura, K. Iwasaki, T. Ido, M. Kojima, J. Koong, R. Kumazawa, H. Kuramoto, T. Minami, I. Nomura, H. Sakakita, M. Sasao. K.N. Sato, T. Tsuzuki. J. Xu, I. Yamada and T. Watari,
Density Fluctuation in JIPP T-IIU Tokamak Plasmas Measured by a Heavy Ion Beam Probe; Nov. 1996

NIFS-462 N. Katsuragawa, H. Hojo and A. Mase,
Simulation Study on Cross Polarization Scattering of Ultrashort-Pulse Electromagnetic Waves; Nov. 1996

NIFS-463 V. Voitsenya, V. Konovalov, O. Motojima, K. Narihara, M. Becker and B. Schunke,
Evaluations of Different Metals for Manufacturing Mirrors of Thomson Scattering System for the LHD Divertor Plasma; Nov. 1996

NIFS-464 M. Pereyaslavets, M. Sato, T. Shimozuma, Y. Takita, H. Idei, S. Kubo, K. Ohkubo and K. Hayashi,
Development and Simulation of RF Components for High Power Millimeter Wave Gyrotrons; Nov. 1997

NIFS-465 V.S. Voitsenya, S. Masuzaki, O. Motojima, N. Noda and N. Ohyabu,
On the Use of CX Atom Analyzer for Study Characteristics of Ion Component in a LHD Divertor Plasma; Dec. 1996

NIFS-466 H. Miura and S. Kida,
Identification of Tubular Vortices in Complex Flows; Dec. 1996

NIFS-467 Y. Takeiri, Y. Oka, M. Osakabe, K. Tsumori, O. Kaneko, T. Takanashi, E. Asano, T. Kawamoto, R. Akiyama and T. Kuroda,
Suppression of Accelerated Electrons in a High-current Large Negative Ion Source; Dec. 1996